Original Research

Mechanisms of cell injury induced by inhaled molybdenum trioxide nanoparticles in Golden Syrian Hamsters

Erin A Huber iD and **Joseph M Cerreta** iD

College of Pharmacy and Health Sciences, St. John's University, Queens, NY 11439, USA
Corresponding author: Joseph M Cerreta. Email: cerretaj@stjohns.edu

Impact Statement

Humans are exposed to nanomaterial occupationally and in everyday life; however, there is a lack of research on the risks and health effects following exposure to many types of nanoparticles. The possible toxicity of MoO₃ NPs has not been studied in a human or an animal model. This study provides a possible mechanism to the toxicological effects of inhaled MoO₃ NPs in Golden Syrian Hamsters. The data from this study suggest that pulmonary exposure to MoO₃ NPs may cause a cell death through pyroptosis following interruption to autophagy. This research shows inhaled MoO₃ NPs exert toxicological effects in the lung, and further studies are needed to evaluate the risk to these particles.

Abstract

Molybdenum trioxide nanoparticles (MoO_3 NPs) are extensively used in the biomedical, agricultural, and engineering fields that may increase exposure and adverse health effects to the human population. The purpose of this study is to evaluate a possible molecular mechanism leading to cell damage and death following pulmonary exposure to inhaled MoO_3 NPs. Animals were separated into four groups: two control groups exposed to room air or aerosolized water and two treated groups exposed to aerosolized MoO_3 NPs with a concentration of $5\,mg/m^3$ NPs (4 h/day for eight days) and given a one-day (T-1) or seven-day (T-7) recovery period post exposure. Pulmonary toxicity was evaluated with total and differential cell counts. Increases were seen in total cell numbers, neutrophils, and multinucleated macrophages in the T-1 group, with increases in lymphocytes in the T-7 group ($*P < 0.05$). To evaluate the mechanism of toxicity, protein levels of Beclin-1, light chain 3 (LC3)-I/II, P-62, cathepsin B, NLRP3, ASC, caspase-1, interleukin (IL)-1β, and tumor necrosis factor-α (TNF-α) were assessed in lung tissue. Immunoblot analyses indicated 1.4- and 1.8-fold increases in Beclin-1 in treated groups (T-1 and T-7, respectively, $*P < 0.05$), but no change in protein levels of LC3-I/II in either treated group. The levels of cathepsin B were 2.8- and 2.3-fold higher in treated lungs (T-1 and T-7, respectively, $*P < 0.05$), the levels of NLRP3 had a fold increase of 2.5 and 3.6 (T-1 $*P < 0.05$, T-7 $**P < 0.01$, respectively), and the levels of caspase-1 indicated a 3.8- and 3.0-fold increase in treated lungs (T-1 and T-7, respectively, $*P < 0.05$). Morphological changes were studied using light and electron microscopy showing alterations to airway epithelium and the alveoli, along with particle internalization in macrophages. The results from this study may indicate that inhalation exposure to MoO_3 NPs may interrupt the autophagic flux and induce cytotoxicity and lung injury through pyroptosis cell death and activation of caspase-1.

Keywords: Molybdenum oxide, nanoparticles, pyroptosis, autophagy, inhalation, pulmonary

Introduction

Free molybdenum (Mo) is a transition metal that occurs naturally in ores such as molybdenite and wulfenite[1,2] that serve as the major sources of the metal.[3] As a result of Mo's high melting point, strength, and the general belief that it is a metal with a lower toxicity, Mo has found use in the military, aeronautical, automobile, and biomedical fields.[1–3] Molybdenum (VI) oxide nanoparticles (MoO₃ NPs) have high ductility and strength at high temperatures, resist corrosion, and are good electrical and thermal conductors.[4] Due to its physical properties, MoO₃ NPs have found use as an additive to lubricants, rubber, filaments in electrical devices, solar cells, and coatings in nanowires.[2,4] They have been used as

an antimicrobial agent against Gram positive bacteria such as *Staphylococcus aureus* and *Bacillus subtilis*.[5]

The broad use of MoO₃ NPs raises a concern of possible adverse health effects in humans as various metal nanoparticles such as tungsten oxide, cobalt oxide, lanthanum oxide, cerium oxide, and carbon nanotubes have been associated with accumulation in tissues and tissue injury.[6–10] Although respiratory exposure to MoO₃ NPs has not been thoroughly studied, the inhalation of Mo compounds has been shown to result in irritation to the respiratory tract, pulmonary hemorrhages, perivascular edema, and damage to the liver and kidneys.[11] A long-term study of occupational exposure to Mo fumes containing MoO₃ has indicated that concentrations between 1 and 19 mg/m³ resulted in the development

of pneumoconiosis.[3,12] In addition, other types of metal nanoparticles have been implicated in pulmonary injury. In a study of cerium oxide nanoparticles, a known occupational and environmental irritant, particles accumulated in the alveoli and interstitial tissue of the lung leading to pulmonary and systemic toxicity.[13] Examination of lung tissue from welders has shown an accumulation of iron, chromium, and manganese nanoparticles along with an increase of macrophages in the alveolar space and fibrotic lesions indicating an inflammatory response.[14] Occupational exposure to WC-Co dusts has been shown to lead to asthma, hard metal lung disease that manifests as progressive inflammation and/or fibrosis, with an increasing risk of cancer.[15] The current exposure guidelines from the Occupational Safety and Health Administration (OSHA) state that the permissible exposure limit (PEL) for an 8-h time weighted average for MoO_3 NPs is $5\,mg/m^3$, with the same guidance from the American Conference of Governmental Industrial Hygienists for a threshold limit value (TLV) for MoO_3 NPs of $5\,mg/m^3$.

Nanoparticles are known to enter the body through various routes with the most common path often being inhalation. To understand the toxic effects of inhaled MoO_3 NPs and to mimic real-life exposure to nanomaterial, a whole-body exposure chamber was utilized in this study. While intratracheal insufflation is a common method in respiratory toxicity studies, a whole-body exposure inhalation system has several advantages. The ECETOC technical report number 122 states that such a system provides a continuous exposure to the nanoparticles, allows particle deposition and clearance in the respiratory tract, and considers the whole respiratory tract. The animal model selected in this study was the Golden Syrian Hamsters (*Mesocricetus auratus*).[16] Golden Syrian Hamsters have been used as models of lung diseases such as pulmonary fibrosis, emphysema, and acute lung injury.[6,17,18] More recently, this animal model has been used to study the sex differences following infection to SARS-CoV-2, along with the development of acute respiratory distress syndrome.[19,20]

Once inhaled, particles may enter the lower respiratory tract and come directly in contact with alveolar epithelium (both Type I and Type II pneumocytes) and macrophages.[21] Inhaled tungsten oxide nanoparticles have been shown to be internalized in the alveolar epithelium and in macrophages, resulting in an acute inflammatory response and tissue damage.[6] Once inside cells, nanoparticles may be capable of interrupting a number of cell pathways that then lead to altered cell function or death. While there are multiple cell death pathways, only a few have been implicated in toxicity following exposure to nanomaterial, that is, apoptosis, oncosis, autophagy, and pyroptosis.[22] Nanoparticles that have been shown to cause apoptotic cell death including particles composed of zinc, copper, titanium, and silica oxide nanoparticles.[22,24] While gold nanoparticles have been shown to cause oncosis in fibroblasts, epithelial cells, and in macrophages.[25]

Autophagy is a conserved process by which faulty organelles and proteins are sequestered in a double-membrane bound vesicle, known as the autophagosome.[26] Autophagy may be a cell preservation mechanism, or alternatively, it can lead to cell death. The process of autophagy can be activated through oxidative stress, from toxins, and damaged cells and/or stressed organelles.[27] Exposure to nanomaterial may stimulate autophagy through the internalization of nanomaterial into the cell.[28] The initiation of autophagy begins with the nucleation of the phagophore with the ULK/Atg1 complex moving and combining with the Beclin-1/phosphoinositide 3-kinase (PI3K) complex.[28–30] Beclin-1 is located in cytoplasmic structures and is needed to localize autophagy-related proteins (ATGs) to preautophagosomal structures.[29] Following nucleation, the phagophore begins to elongate to form the autophagosome. The elongation step is mediated by Atg12 conjugation system and microtubule-associated protein 1A/1B light chain 3 (LC3) – conjugation system.[29,31] LC3 is located in the cell's cytoplasm and contains two isoforms, LC3-I and LC3-II. Once activated, LC3-I is transferred to Atg3, which is an E2-like carrier protein that will allow the conversion of LC3-I to the phosphatidylethanolamine-conjugated form known as LC3-II.[31] LC3-II is considered the biomarker for autophagosome formation.[27,29] Finally, the autophagosome will fuse with the lysosome to form the autolysosome, where contents located in the inner compartment, including LC3-II, will be degraded.[28,29,31] During the process of autophagy, interruptions or impairments can occur anywhere from the initiation of the phagophore to the formation of the autolysosome.[32] Impairments in such autophagic flux can be monitored through the protein P-62, also known as SQSTM1/sequestosome-1.[32] P-62 is degraded in the autolysosome as it is a selective substrate that binds to LC3-II in the autophagosome.[27] Studies have shown activation of autophagy may be followed by an impairment in autophagic flux following nanoparticle exposure. Copper, silica, silver, and zinc oxide nanoparticles, along with rare-earth oxide nanoparticles such as lanthanum, have been shown to cause autophagic flux interruption.[26,33–36]

If autophagic flux is interrupted, other pathways may be implicated in cell injury. Pyroptosis is a cell death pathway dependent on caspase-1 activation resulting in an inflammatory response through the conversion of pro-interleukin (IL)-1β to active IL-1β.[37] Following tissue injury and/or exposure to engineered nanoparticles, caspase-1 may be activated as a result of danger signals in the cell's cytosol through nod-like receptors (NLRs).[37,38] The NLR family pyrin domain-containing 3 (NLRP3) can form a multiprotein complex known as the inflammasome as a result of such danger signals.[37] During activation of the NLRP3 inflammasome, NLRP3 will interact with apoptosis-associated speck-like protein containing a CARD (ASC) pyrin domain. The CARD domain on ASC will then recruit the CARD domain on pro-caspase-1 that will in turn form the NLRP3 inflammasome.[24] After the formation of the NLRP3 inflammasome, pro-caspase-1 will be converted to active caspase-1 and IL-1β will then undergo caspase-1-dependent activation.[37] The NLRP3 inflammasome can be activated although changes in the ion fluxes, such as K^+ efflux, generation of reactive oxygen species (ROS), and cathepsin B release.[24] The inefficient clearance of particulate matter may lead to lysosomal destabilization through the rupture of the lysosome and subsequent release of cathepsin B.[24] Inhalation exposure to tungsten oxide nanoparticles in Golden Syrian Hamsters has been shown to activate the NLRP3 inflammasome through cathepsin B release.[6] Other nanoparticles have been shown to activate the

NLRP3 inflammasome as a result of lysosomal destabilization and cathepsin B release, that is, cerium oxide nanorods, rare-earth oxide nanoparticles (La_2O_3 NPs), and fumed silica nanoparticles.[26,36,39]

While autophagy is considered a protective mechanism, an over exposure to nanomaterial may disrupt the homeostatic balance, leading to mitochondrial and lysosomal dysfunction and eventual cell death.[26] Exposure to nanomaterial may stimulate autophagy; however, such materials may block the formation of the autolysosome through a loss of lysosomal integrity.[28] Silica, copper oxide, silver, and zinc oxide nanoparticles are known to interrupt autophagic flux through destabilization of the lysosome caused by interference in lysosomal acidification or permeabilization of the lysosome's membrane.[26,33–35] Autophagy is able to remove activated NLRP3 inflammasome complexes, but a disturbance in the autophagic flux might prevent the removal of the complex and lead to exaggerated levels of IL-1β.[36]

The aim of this study is to determine the molecular mechanism leading to cell injury and death following exposure to inhaled MoO_3 NPs in Golden Syrian Hamsters. The hypothesis for this study is that exposure to inhaled MoO_3 NPs will deposit and internalize in respiratory epithelium and alveolar macrophages, interrupting autophagic flux that leads to the activation of the NLRP3 inflammasome, causing an inflammatory response, cell damage, and cytotoxicity.

Materials and methods

MoO_3 NPs were purchased from Nanostructured & Amorphous Materials, Inc (Katy, TX, USA). Dulbecco's phosphate buffered saline was obtained from Gibco, Thermo Fisher Scientific (Waltham, MA, USA). RPMI-1640 Medium was purchased from Cytiva, HyClone Laboratories (Logan, UT, USA). Nanosphere™ Size Standards, Pierce™ BCA Protein Assay Kit, PROTOCOL® Hema 3® Stain Set, and Zeta Potential Standard were obtained from Thermo Fisher Scientific. Laemmli Sample Buffer, Mini-PROTEAN TGX Gels (7.5%, 12%, and 4–20%), Non-fat dry milk, and Precision Plus Protein™ Dual Color Standards were purchased from Bio-Rad Laboratories, Inc. (Hercules, CA, USA). MagicMark XP Western Protein Standard was purchased from Invitrogen, Thermo Fisher Scientific (Carlsbad, CA, USA). Amersham™ ECL™ Prime Western Blotting Detection Reagents were purchased from Global Life Sciences Solutions Operations UK Ltd., Cytiva (Buckinghamshire, UK). Antibodies against Beclin-1 (mAb), β-actin (mAb), caspase-1 (mAb), cathepsin B (mAb), LC3-I and II (mAb), NLRP3 (mAb), and P-62 (mAb) were purchased from Cell Signaling Technology, Inc. (Danvers, MA, USA). IL-1β enzyme-linked immunoassay (ELISA) Kit and tumor necrosis factor-α (TNF-α) ELISA Kit were obtained from Abcam (Waltham, MA, USA). Mouse PYCARD/ASC/TMS1 ELISA Kit was obtained from LifeSpan BioSciences, Inc. (Seattle, WA, USA).

Nanoparticle characterization

To determine the primary particle size of MoO_3 NPs, an aqueous suspension of MoO_3 NPs was loaded on formvar-coated copper grids, and measured using transmission electron microscopy (TEM) (JEOL JEM-1200EX, Tokyo, Japan). TEM micrographs were analyzed using ImageJ software (version 1.47a). Nanosphere™ Size Standards with a mean diameter of $100\,nm \pm 4\,nm$ were used as a calibration standard for measurements. The mean hydrodynamic diameter of MoO_3 NPs in water was determined by dynamic light scattering (DLS) using a Delsa Nano C Particle Size Analyzer (Beckman Coulter Inc., Brea, California, USA). The zeta potential of MoO_3 NPs was measured using the Malvern Zetasizer Nano ZS (UK). A zeta potential standard ($-42 \pm 4.2\,mV$) was used as a calibration standard for the instrument.

Animals

Female Golden Syrian Hamsters (seven to eight weeks of age) were obtained from Envigo (Indianapolis, IN, USA). Animals were housed under a controlled environment with a 12-h light–dark cycle and were provided a standard laboratory diet and water *ad libitum*. All animal experiments were carried out under an Institutional Animal Care and Use Committee (IACUC) approved protocol.

Experimental design

Golden Syrian Hamsters were divided into four groups: Group 1: exposed to only room air group (no exposure), Group 2: exposed to sterile aerosolized water for 4 h/day for eight days (Control) in a whole-body exposure chamber (CH Technologies Inc., NJ, USA), Group 3: exposed to 5 mg/m^3 MoO_3 NPs for 4 h/day for eight days euthanized one-day post exposure (T-1), and Group 4: exposed to 5 mg/m^3 MoO_3 NPs for 4 h/day for eight days euthanized seven days post exposure (T-7). The concentration of 5 mg/m^3 was selected as it represents the PEL and TLV for OSHA and American Conference of Governmental Industrial Hygienists (ACGIH), respectively. An eight-day exposure to inhaled MoO_3 NPs was selected as previous research on inhaled tungsten oxide nanoparticles in Golden Syrian Hamsters utilized this duration to determine the molecular mechanism of toxicity.[6]

Aerosols were generated using an eight jet nebulizer (CH Technologies, Inc., NJ, USA) attached to a collision jar that was supplied with compressed air. MoO_3 NP suspensions were prepared in sterile distilled water and sonicated overnight. To track the concentration of particles in the chamber, samples of the air containing MoO_3 NPs were then diluted (1:100) in a particle diluter (Model 3332) (TSI Inc., MN, USA) and then measured for the mass aerosol concentration (mg/m^3) every minute for the entire duration of exposure using a NanoScan® scanning mobility particle sizer (SMPS) 3910 (TSI, Inc.).

Analysis of bronchoalveolar lavage fluid

Following euthanasia, a catheter was inserted in the trachea and lungs were lavaged with sterile ice cold Dulbecco's phosphate buffered saline ($CaCl_2$ and $MgCl_2$ free) (DPBS, pH 7.4). Aliquots of bronchoalveolar lavage fluid (BALF) were pooled, centrifuged, cellular fractions were resuspended, and total cell count was determined. BALF smears were prepared using cytocentrifugation, stained, and the differential cell count made. Cells were categorized as macrophages, multinucleated macrophages, neutrophils, lymphocytes,

and eosinophils. A total of 1000 cells were counted per slide, and the results were presented as percentages of various cell types.

Light microscopy

Lungs were fixed *in situ* by insufflation with 10% neutral buffered formalin. Following fixation, lungs were removed and fixed for an additional three days. Fixed tissue was serially dehydrated using increasing concentrations of ethanol, cleared in xylene, and embedded in Paraplast® X-TRA. Tissue blocks were cut to yield a tissue section thickness of 4–6 μm, sections were mounted on glass slides, stained with hematoxylin & eosin, and examined using an Olympus BH-2 microscope.

Electron microscopy

Tissue and cells were also examined by scanning electron microscopy (SEM) and TEM after exposure to MoO_3 NPs. Lungs from hamsters were fixed *in situ* by insufflation with 3% glutaraldehyde. For SEM, samples were washed in buffer, dehydrated to 100% acetone, and dried using the critical point method. Samples were mounted on aluminum stubs, sputter coated with platinum/palladium, and examined using a scanning electron microscope (JEOL JSM 6010LA).

For TEM, fixed tissue blocks were postfixed in 1% osmium tetroxide for 1 h, stained with 0.5% uranyl acetate, dehydrated in acetone, and embedded 100% LX-112-araldite resin mixture. Tissue blocks were sectioned and sections were stained with uranyl acetate and lead citrate. Tissue sections were examined using a JEOL JEM-1200EX TEM.

Immunoblot analyses

Lung tissue was washed with DPBS, snap frozen, and stored in liquid nitrogen until use. Lung tissue homogenates were prepared using radioimmunoprecipitation assay (RIPA) lysis buffer containing a protease and phosphatase inhibitor cocktail. Samples were denatured at 95°C for 5 min in Laemmli sample buffer containing 5% (v/v) beta-mercaptoethanol, and separated using electrophoresis. Resolved proteins were transferred to polyvinylidene difluoride (PVDF) membrane, blocked with 5% (w/v) non-fat dry milk in Tris-Buffered Saline (TBST), washed with TBST and incubated with the respective primary antibody for 3 h or overnight at 4°C. The following primary antibodies were used: Beclin-1 (1:1000), caspase-1 (1:1000), cathepsin B (1:1000), LC3-I/II (1:1000), NLRP3 (1:1000), and P-62 (1:1000). A horseradish peroxidase (HRP)-linked secondary antibody (1:1000) was used to probe the membranes and an anti-IgG β-actin (1:5000) was used to measure actin, that was used as a loading control. Following primary antibody incubations, membranes were washed with TBST, and then incubated with the secondary antibody for 2 h. Chemiluminescence was detected using Amersham™ ECL™ Prime Western Blotting Detection Reagent (GE Healthcare, Bukinghamshire, UK) and membranes were photographed using Alpha Innotech digital imager (Alpha Innotech Corp., San Leandro, CA, USA). Images were analyzed by densitometry using Image J software (version 1.47a).

ELISAs

ASC/PYCARD/TMS1, IL-1β, and TNF-α levels were determined in lung samples from control and treated animals using the sandwich ELISA technique kits. Lung homogenate preparation and determination of protein concentrations were described above. Concentration of lung homogenate was determined based on the manufacturer's protocol. The respective proteins were detected following incubation with a biotinylated antibody, after incubation with streptavidin-HRP, and finally detected with the addition of the TMB substrate. The absorbance was measured at 450 nm. Protein levels were calculated from the generated standard curves.

Statistical analysis

Statistical analyses were carried out using GraphPad Prism® version 5.0 (La Jolla, CA, USA). Significance tested between two groups used an unpaired *t*-test. Significance tested between groups used one-way analysis of variance (ANOVA) followed by the Newman–Keuls multiple comparison post hoc test. The results are expressed as mean value ± standard error of mean. Data were considered to be significant at the 95% confidence level ($P < 0.05$) and noted based on the ranking *$P < 0.05$, **$P < 0.01$, and ***$P < 0.001$.

# Results

Nanoparticle characterization

MoO_3 NPs were characterized using TEM to determine particle size (Figure 1(a)), DLS to determine the hydrodynamic diameter (Figure 1(b)), and the zeta potential (Figure 1(c)). The average particle size of MoO_3 NPs was determined by randomly selecting TEM micrographs and averaging the particle size of 100 individual MoO_3 NPs. Individual particles were observed to have a spherical shape and despite sonication particles still agglomerated and/or aggregated. The average particle size of MoO_3 NPs was determined to be 33 nm. An additional electron micrograph of individual MoO_3 NPs can be seen in Supplementary Figure 1. To validate measurements, the Nanosphere™ size standards (102 ± 3 nm) were used as an internal control. The hydrodynamic diameter of MoO_3 NPs in water (526 nm) was determined using DLS. The zeta potential of MoO_3 NPs was found to be -54.4 ± 7.7 mV.

BALF analyses

Golden Syrian Hamster were exposed to 5 mg/m³ MoO_3 NPs for 4 h per day for eight days and given a recovery period post exposure of either one day (T-1) or seven days (T-7) prior to euthanasia. Data from the cell counts and immunoblot analyses from no exposure controls are not presented, as the number of cells and protein levels did not differ from the control data from lungs of animals exposed to the vehicle of water. Samples of the BALF from hamsters exposed to MoO_3 NPs were assessed for changes to the cell numbers and for inflammation within the lung. Total cell counts were significantly changed in the BALF of hamsters in the T-1 group
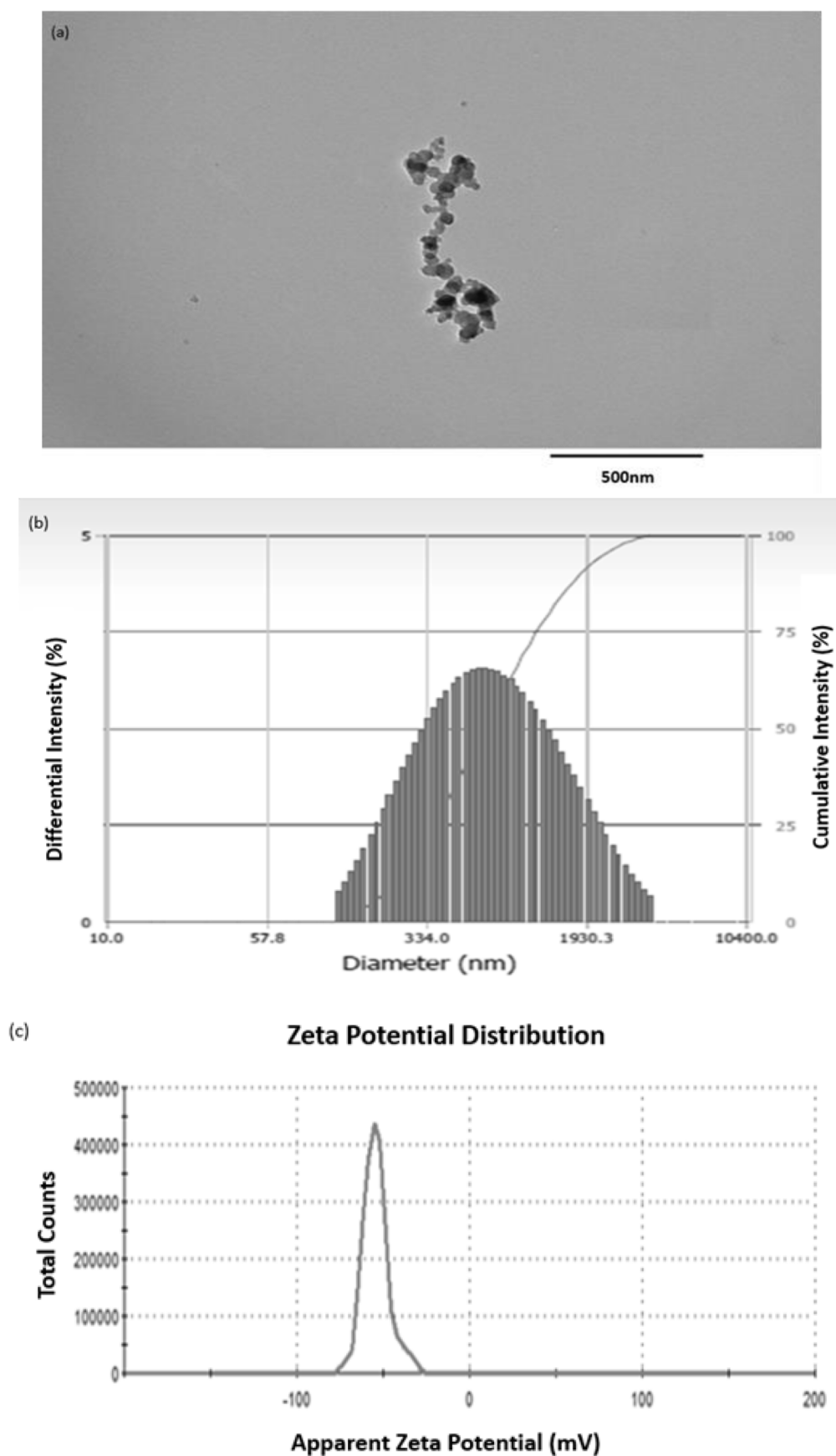
Figure 1. MoO$_3$ NPs were characterized using TEM, DLS, and the zeta potential. (a) The electron micrograph with an original magnification ×25,000 of an aqueous suspension of MoO$_3$ NPs on formvar coated copper grids. The average particle size was determined to be 33 nm as compared to a known standard. (b) Distribution of particle size in an aqueous suspension of MoO$_3$ NPs in H$_2$O using DLS. The average hydrodynamic diameter was determined to be 526 nm. (c) Representative zeta potential distribution of an aqueous suspension of MoO$_3$ NPs in H$_2$O. The zeta potential was determined to be −54.4 ± 7.7 mV.
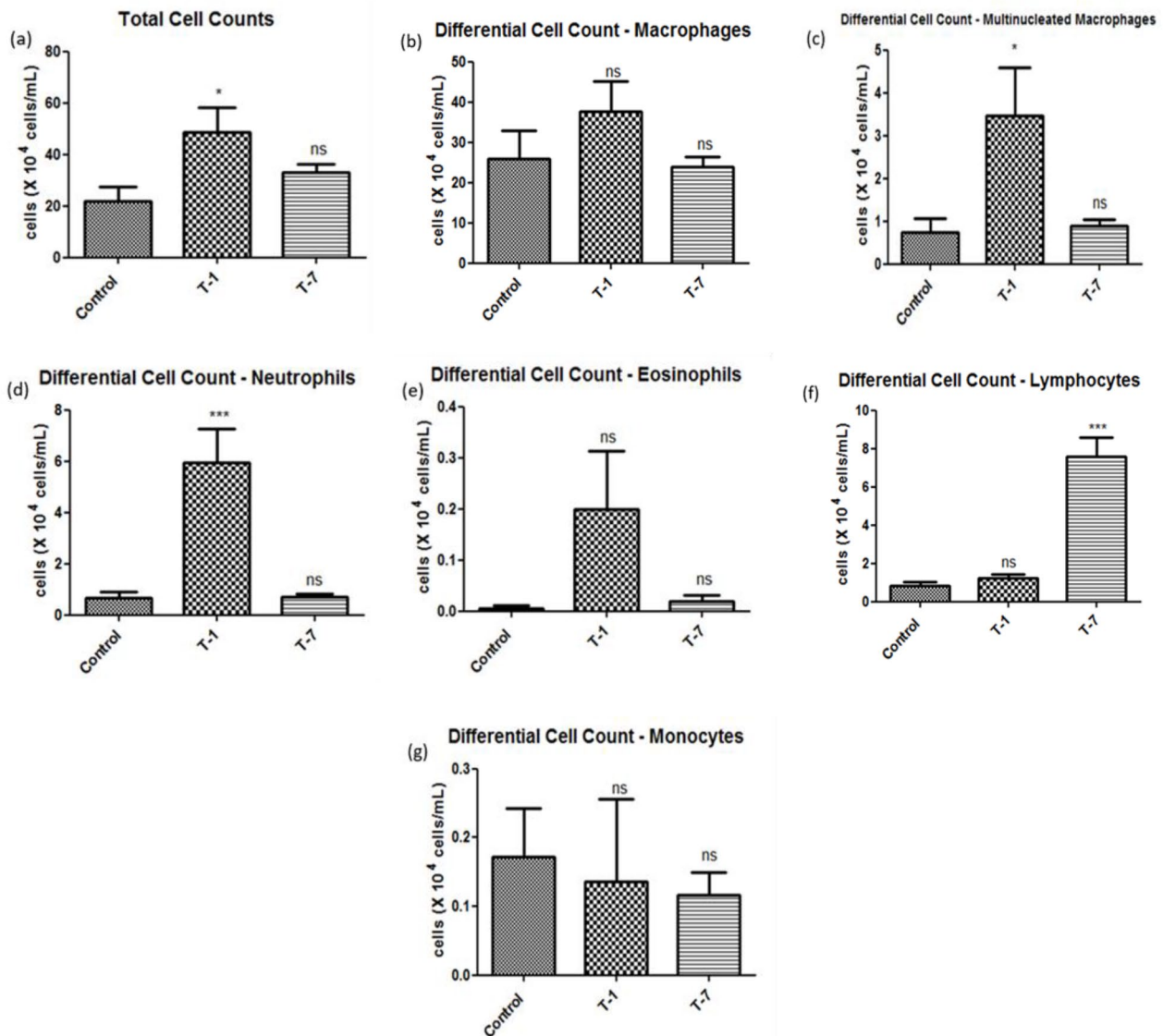
Figure 2. These graphs represent the changes to the cell types in the bronchoalveolar lavage fluid from animals exposed to 5 mg/m³ MoO₃ NPs, collected one day (T-1) or seven days (T-7) post exposure. Cellular fractions were resuspended in 1 mL of RPMI-1640 media and (a) total cell counts were determined. The total cell count was significantly increased (1.7-fold higher) in the T-1 group when compared to the controls. Differential cell counts were carried out on leukocytes in the BALF. Animals in the T-1 group had significant increases in multinucleated macrophages (c) (*$P < 0.05$, 4.7-fold) and in neutrophils (d) (***$P < 0.001$, 8.7-fold) compared to the controls. T-7 animals had a statistically significant increase in lymphocytes (f) (***$P < 0.001$, 9.4-fold) when compared to the control.

(Figure 2(a)). Differential cell counts indicated no significant change in counts of pulmonary macrophages (Figure 2(b)) in animals exposed to 5 mg/m³ MoO₃ NPs when compared to controls. There was a significant increase in multinucleated macrophages (Figure 2(c)) by 3×10^4 cells/mL and in neutrophils (Figure 2(d)) by 5.94×10^4 cells/mL in the T-1 group when compared to controls. Numbers of eosinophils (Figure 2(e)) were not significantly altered when compared to controls. Animals in the T-7 group had a significant increase in lymphocytes (Figure 2(f)) by 7.60×10^4 cells/mL when compared to the controls. Counts of monocytes (Figure 2(g)) were not significantly altered in either treated groups. Photomicrograph of cytosmears of the BALF from hamsters in the T-1 group shows immature neutrophils, band cells, as indicated by the black arrow and multinucleated

macrophages indicated by the black triangles as shown in Supplementary Figure 2(a).

Histopathological examination of lung tissue

Histopathological examination of lung tissue sections from both groups of animals exposed to 5 mg/m³ MoO₃ NPs revealed airway epithelial hyperplasia, cell surface membrane blebbing of epithelial tissue in airways, and abnormal growths of epithelial cells in the alveoli. Lung tissue sections from control animals were unremarkable (Figure 3(a)). Lung sections from hamsters in the T-1 group had hyperplastic regions in the airway epithelium and blebbing of epithelial cells (Supplementary Figure 3(a)), while T-7 animals (Figure 3(b)) had hyperplastic regions in the airway epithelium.
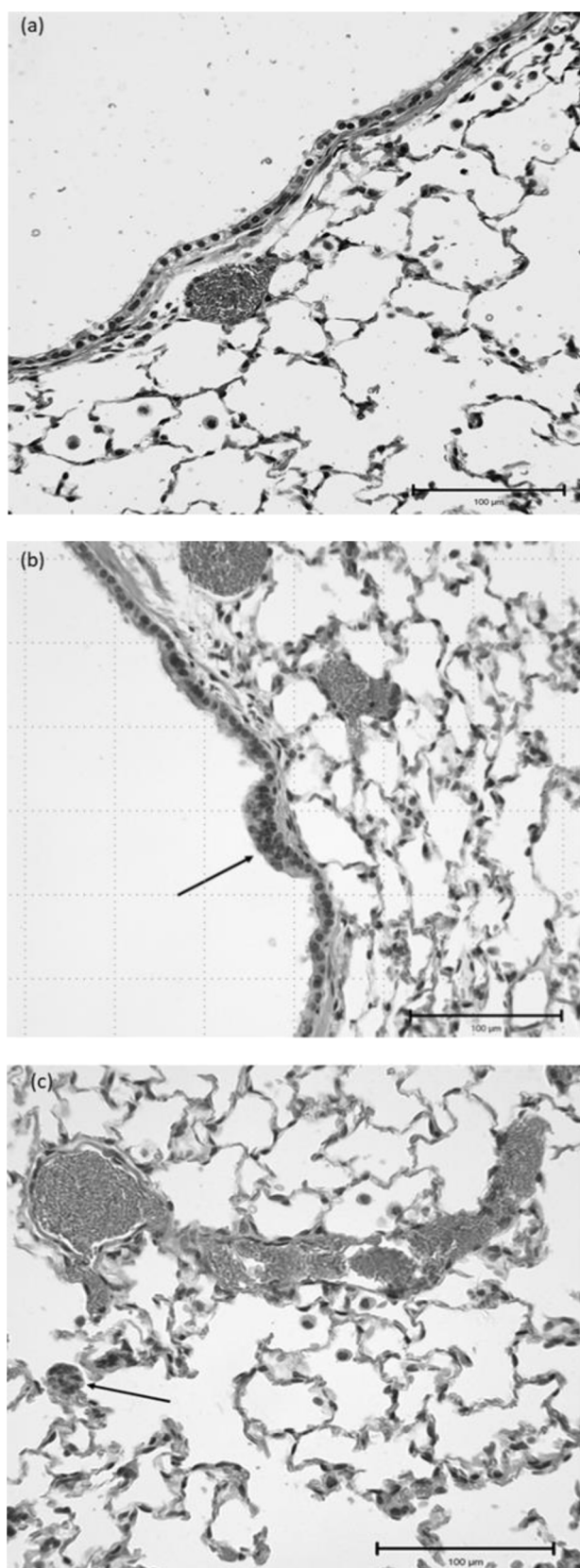
Figure 3. Representative photomicrographs of formalin fixed lung tissue sections from (a) airways of control animals and (b) airways of animals in the T-7 group. H&E stained tissue sections of airway epithelium show focal hyperplasia as indicated by the black arrows (b). (c) Alveoli of hamsters in the T-7 group as seen in. Alveoli (c) of nanoparticle-treated animals show abnormal masses of epithelial tissue as indicated by the black arrow. Original magnification ×400.

Control tissue sections of the alveoli (Supplementary Figure 3(b)) contain simple squamous epithelium along with capillaries within the alveolar septa. In contrast, the T-7 recovery group had abnormal masses of epithelial cells in the alveoli (Figure 3(c)).

SEM was utilized to determine surface morphology following exposure to $5\,mg/m^3$ MoO_3 NPs. Control animals (Figure 4(a)) lacked alterations to airway epithelium with a flat epithelial surface containing minimal membrane blebbing and evenly distributed cilia. SEM photomicrographs from animals in the T-1 group had membrane blebbing on the surface of airway epithelium along with an increased presence of mucus (Figure 4(b)). Membrane blebbing on the surface of airway epithelium was also present in animals in the T-7 group.

TEM was utilized to determine morphological alterations to the cells of the lung following exposure to MoO_3 NPs. Animals in the control groups (Supplementary Figure 5(a)) had alveoli showing cuboidal Type II pneumocytes containing lamellar bodies with intact lamella and surface microvilli. Other portions of the alveolar surface contain squamous Type I Pneumocytes that were unremarkable, while the interstitial region contained capillaries with numerous erythrocytes and squamous endothelial cells. Hamsters in the T-7 group (Figure 5(a)) had damaged Type II Pneumocytes containing vacuoles that lacked lamellae. Abundant collagen was seen in the interstitium of the alveolar septa. MoO_3 NPs were seen in vacuole-like spaces of macrophages from the T-7 group (Figure 5(a) insert). Pulmonary macrophages in the T-1 group (Figure 5(b)) had double-membrane vesicles that appear to be autophagosomes.

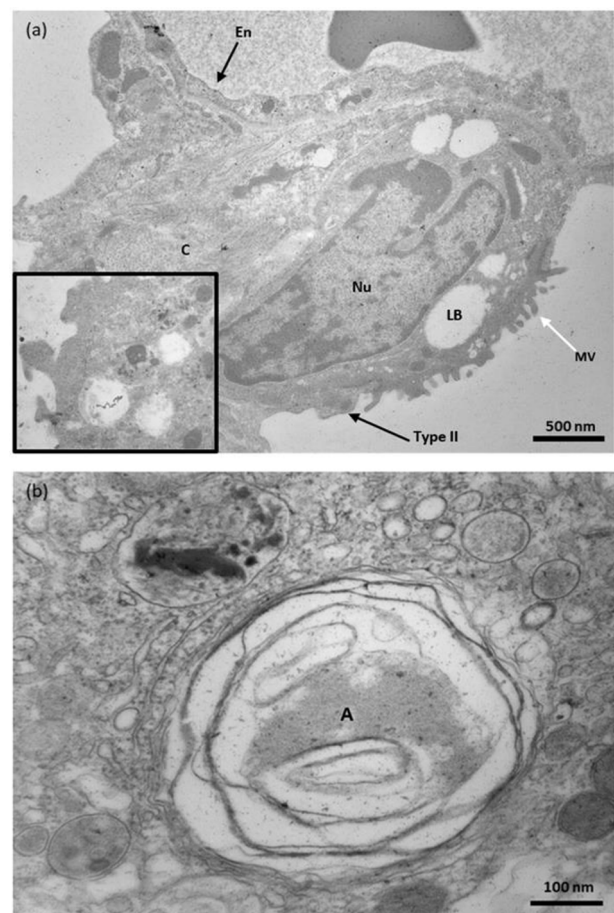### Induction of autophagy and pyroptosis

Golden Syrian Hamsters were treated as described above to study the mechanism of cell injury in following inhaled exposure to MoO_3 NPs. Three pathways were examined, apoptosis, autophagy, and pyroptosis. Previous work in our lab investigated apoptosis in cultured rat pleural mesothelial cells (RPMCs) treated with MoO_3 NPs. Unpublished data from our lab showed no significant change in the levels of caspases-3, 8, and 9 in RPMCs exposed to MoO_3 NPs when compared to vehicle-treated cells. Lung tissue sections from animals exposed to $5\,mg/m^3$ MoO_3 NPs had numbers of TUNEL positive cells that were similar to control groups. The protein Beclin-1 is responsible for the initiation of autophagy. There was a significant increase in Beclin-1 (Figure 6(a)) levels in lungs tissue of animals exposed to $5\,mg/m^3$ MoO_3 NPs (T-1: 1.4-fold, T-7: 1.8–fold, $P < 0.05$) when compared to the controls. LC3 is divided into two isoforms known as LC3-I and LC3-II. LC3-I is converted to form the conjugated LC3-II, known as the biomarker for autophagosome formation. The protein levels of LC3-I (Figure 6(b)) in animals exposed to $5\,mg/m^3$ MoO_3 NPs had no significant change when compared to the controls. The expression levels of LC3-II (Figure 6(c)) in the lung tissue were not significantly increased in either of the treated groups when compared to the controls. An additional immunoblot used for the detection and quantification of LC3-I/II can be seen in Supplementary Figure 6. The protein P-62 is used to monitor autophagic flux as it is
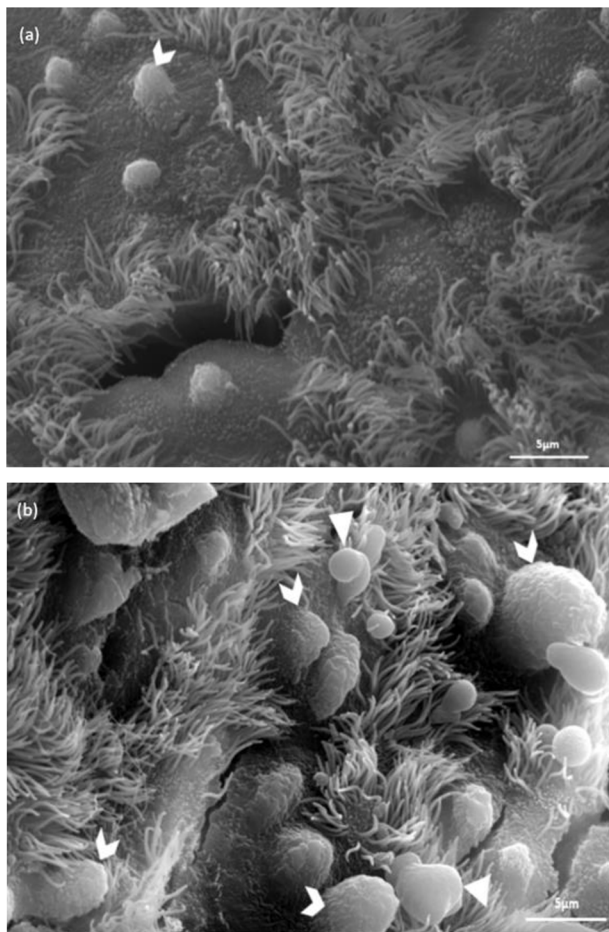
Figure 4. Representative scanning electron photomicrographs of lung tissue fixed in 3% glutaraldehyde from control and animals exposed to 5 mg/m³ MoO₃ NPs. (a) Surface airway epithelium of control animals showing a flat epithelial surface with cilia and minimal membrane blebs as indicated by the arrowhead. (b) The surface of the airway epithelium exposed animals in the T-1 group showing extensive membrane blebbing as indicated by the arrowheads and mucus production as indicated by the triangles. Original magnification ×3300.

Figure 5. Representative transmission electron photomicrographs of lung tissue fixed in 3% glutaraldehyde from animals exposed to 5 mg/m³ MoO₃ NPs. (a) The micrograph from an animal in the T-7 group depicts a Type II pneumocyte as indicated by the black arrow showing damaged lamellar bodies (LBs). The presence of collagen (C) can also be seen in the interstitium. (Original magnification ×10,000). The insert shows internalized MoO₃ NPs as indicated by the black arrow within a vacuole-like structure. (c) Depicts an autophagosome (A) containing a double-membrane vesicle in a macrophage from an animal in the T-1 group. (Original magnification ×50,000).
Type II: Type II pneumocyte; A: autophagosome; Cap: capillary; C: collagen; En: endothelial cell; LB: lamellar body; MV: microvilli; Nu: nucleus.

degraded in the autolysosome. Protein levels of P-62 (Figure 6(d)) were significantly increased in lung tissue of animals in the T-7 group by 1.8-fold ($P < 0.05$) when compared to the controls.

The activation of the inflammasome is the hallmark of pyroptosis. Such activation is indicated by the release of the proteins belonging to the proenzyme family of cathepsin. A disruption in the autophagic flux may lead to lysosomal destabilization and a release of cathepsin B. The protein expression of cathepsin B (Figure 6(e)) was significantly increased in both groups exposed to 5 mg/m³ MoO₃ NPs (T-1: 2.8-fold, T-7: 2.3–fold, $P < 0.05$) when compared to the controls. Once NLRP3 is activated, the NLRP3 inflammasome is formed. The NLRP3 inflammasome contains the proteins: NLRP3, ASC, and pro-caspase-1. Protein expression of NLRP3 (Figure 6(f)) was significantly increased in lung tissue of animals in both treated groups (T-1: 2.5-fold, T-7: 3.6–fold, $P < 0.05$) when compared to the controls. The levels of ASC (Figure 6(g)) were increased when compared to controls. The protein expression of caspase-1 (Figure 6(h)) was increased in animals exposed to 5 mg/m³ MoO₃ NPs

(T-1: 3.8-fold, T-7: 3.0-fold ($P < 0.05$)) when compared to the controls. The formation of the NLRP3 inflammasome can be confirmed from the presence of active caspase-1 as pro-caspase-1 is cleaved to form the active protein. The levels of IL-1β (Figure 6(i)) were significantly increased ($P < 0.01$ and $P < 0.001$) in both groups treated with 5 mg/m³ MoO₃ NPs, by 42.0 pg/mL (T-1) and 42.8 pg/mL (T-7) when compared to the controls.

The levels of TNF-α were investigated in lung tissue of hamster exposed to 5 mg/m³ MoO₃ NPs as it is a pro-inflammatory cytokine. The levels of TNF-α (Figure 6(j)) were significantly increased ($P < 0.05$) in lung tissue of animals in the T-7 group by 1160 pg/mL (2.6-fold increase) when compared to the controls.

Discussion

Golden Syrian Hamsters were used as an animal model. Golden Syrian Hamsters are a suitable model when studying
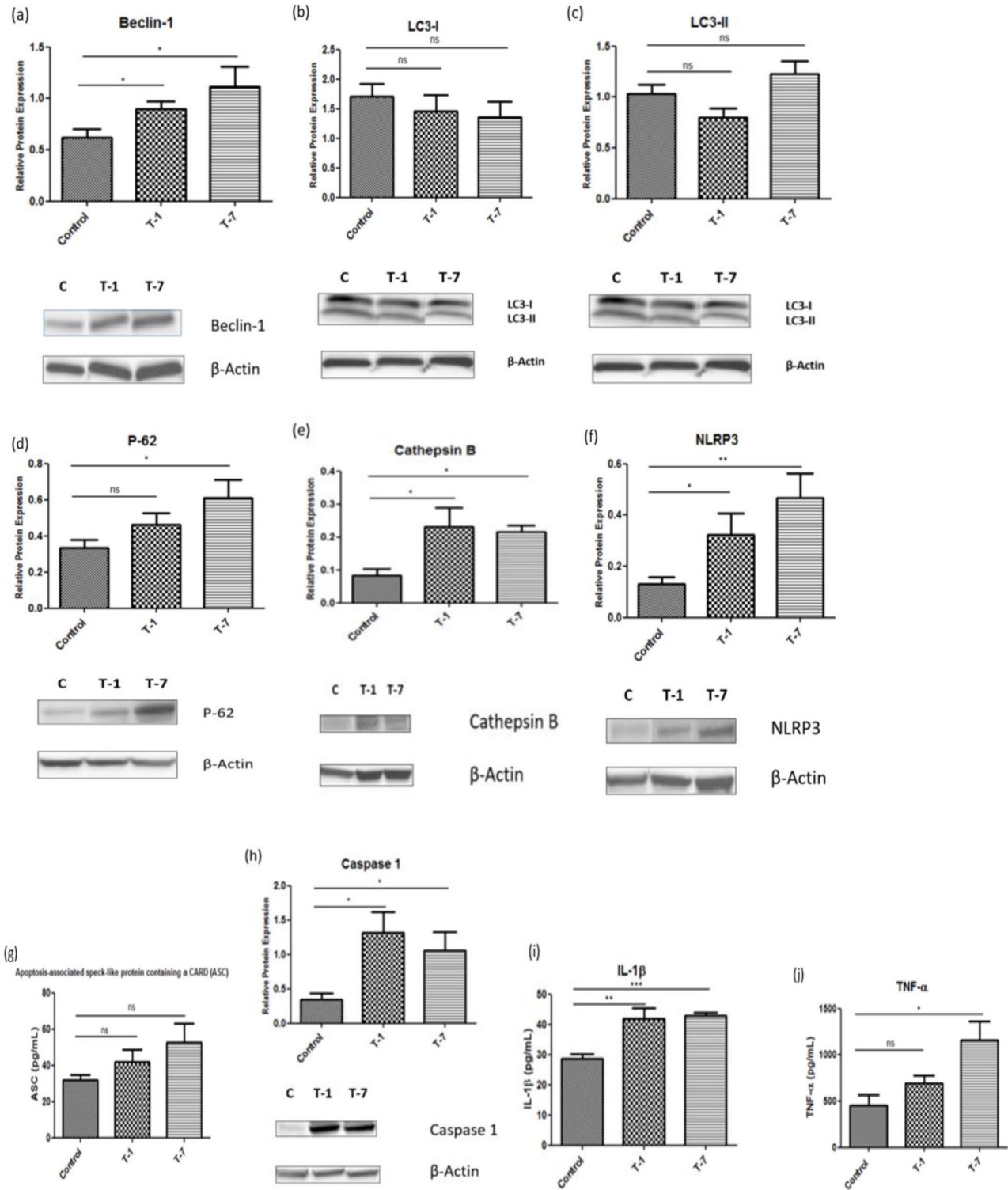
Figure 6. The histograms represent the densitometric analysis of immunoblot for the detection and quantification of proteins associated with autophagy ((a)–(d)) and histograms ((e), (f), and (h)) for proteins associated with the inflammasome pathway. Histograms ((g), (i), and (j)) represent the ELISA analyses of proteins associated with the inflammasome pathway and inflammation. The relative protein expression for animals in the T-1 and T-7 groups had fold increases for (a) Beclin-1 (1.4 and 1.8, respectively), (d) P-62 (unchanged and 1.8, respectively), (e) cathepsin B (2.8 and 2.3, respectively), (f) NLRP3 (2.5 and 3.6, respectively), (g) ASC (1.3 and 1.7, respectively), (h) caspase-1 (3.8 and 3.0, respectively), (i) IL-1β (1.5 and 1.5, respectively), and (j) TNF-α (1.6 and 2.6, respectively); there was no significant change in protein levels of (b) LC3-I and (c) LC3-II in both treated groups. Representative immunoblots for the respective proteins that are normalized to β-actin are found below the histograms.

the lung as these animals rarely develop spontaneous pneumonia[40] and have an immune response comparable to that of a human.[6,16] An additional benefit of this animal model is that Golden Syrian Hamsters are an outbred model that will allow more genetic diversity in disease modeling than would be in mice.[41] Inbred strains of mice and rats have been shown to have strain-dependent susceptibility to inhaled materials such as cigarette smoke and nanomaterial such as Quantum Dots.[6]

Physical characterization is important in studies of nanomaterial to understand how the particle physically and chemically interacts in a biological medium. In inhalation studies, the size of a nanoparticle is of importance as it can impact the area of deposition in the lung,[42–44] the method of endocytosis, and their internalization within the tissue.[28,39] In this study, MoO_3 NPs were characterized using TEM and DLS to determine particle size and the zeta potential. Nanomaterials were characterized in both a dry and wet state as the dry state will provide information on the size and surface area and the wet state will determine the size distribution and aggregation potential in a relevant media.[45,46] In the dry state of MoO_3 NPs had an average particle size of 33 nm as determined by TEM while MoO_3 NPs in water had a hydrodynamic diameter of 526 nm determined by DLS. The hydrodynamic diameter of nanoparticles is commonly larger in size when compared to particle size using TEM as the latter technique can detect agglomerate and characterize samples with broad size distributions.[46] Differences in the dry and wet state size of NPs have been seen in various nanoparticle studies with other materials such as Al, Cu, Si, W oxide,[6,46] and carbon nanotubes. Such studies have shown that particles do not retain their nanoscale size when measured using DLS. The zeta potential of MoO_3 NPs in water was measured to be -54.4 ± 7.7 mV making this a stable suspension with an anionic surface charge on the particle.[47,48]

"Health Effects Test Guidelines" (OPPTS 870.1300) from the US EPA on acute inhalation toxicity were followed. Measurements that were monitored during the exposure were the rate of airflow, continuous monitoring of a steady concentration of the test substance, and measurement of the particle size. This study monitored the aerosolized MoO_3 NPs suspension with samples of air taken every minute during the duration of the exposure and analyzed using a NanoScan® SMPS. The aerosolized suspension of MoO_3 NPs had an average geometric mean particle diameter of 65 nm and a particle diameter range between 12 and 154 nm. This increase in size may be attributed to the nanoparticle's ability to form aggregates or agglomerates once aerosolized within the chamber as was seen in another study[6] using tungsten oxide nanoparticles. The increase in particle size when monitored using the SMPS may support the increase in size when MoO_3 NPs were analyzed using DLS, compared to TEM measurements. As a result of the properties of nanomaterials, these particles will agglomerate and/or aggregate, and will show heterogenicity in particle size. The various sizes of the nanoparticles reported here are the result of how they were measured. For TEM, the particles are in a dry state; for DLS, the particles are in a liquid environment; and in the NanoScan® SMPS, the particles are aerosolized. Particle interaction with their environment will affect their size. The size of the particles that were aerosolized and monitored using the NanoScan® SMPS may be more relevant as this is the state the particles were in when inhaled by experimental animals.

Golden Syrian Hamsters were exposed to 5 mg/m³ MoO_3 NPs as this concentration represents the PEL for an 8-h time weighted average from OSHA and the TLV from ACGIH. Hamsters were exposed to MoO_3 NPs for 4 h per day as this is an OECD guideline for inhalation toxicity studies. Animals were then exposed for a continuous eight days to study the molecular mechanism leading to toxicity from inhaled nanoparticles.[6] Following eight days of exposure to MoO_3 NPs, animals in the T-1 group were utilized to investigate the acute inflammatory response following exposure to these particles, while animals in the T-7 group were used to evaluate a continuation of the inflammatory response and the possibility of changes to the lung tissue indicating a fibrotic process.

MoO_3 NPs were used to study the toxic effects of inhaling such particles into the lungs of Golden Syrian Hamsters through activation of autophagy, or attenuates the induction of the NLRP3 inflammasome leading to pyroptosis with the release of inflammatory cytokines. Exposure to nanomaterial can elicit an acute and/or chronic inflammatory response. Total cell counts from the BALF were significantly increased in the T-1 group that could suggest an inflammatory response was initiated after inhaling MoO_3 NPs. Total cell counts from the BALF were used as an indicator to determine the degree of the inflammatory response in the lung following exposure to nanomaterial.[8] BALF from animals in the T-1 group had a significant increase in the number of neutrophils and multinucleated macrophages while animals in the T-7 group had a significant increase in lymphocytes. The acute inflammatory response is characterized by the induction of polymorphonuclear leukocytes (PMN), and these cells will remain in the lung for a few days.[49] If the inflammatory response does not fully resolve, macrophages will replace PMNs and lymphocytes may accompany the response.[49] An increase in neutrophils reflects an acute inflammatory response in the 5 mg/m³ MoO_3 NPs group given a one-day recovery period post exposure and that response shifted to a more chronic inflammatory response following seven days of recovery as suggested by the increase in lymphocytes. Formation of multinucleated macrophages following exposure to nanomaterial may in part be a result of oxidative stress.[23] The cytokine TNF-α is known to play a role in the regulation of the immune system, but overexpression of this protein may lead to a chronic inflammatory response or cell death through pro-inflammatory signaling.[50] Lung tissue from animals in the T-7 group had a significant increase in levels of TNF-α, suggesting a continuation of the inflammatory response after exposure to MoO_3 NPs had ceased. The internalization of inhaled nanoparticles may result in lung injury mediated by a pro-inflammatory response. Macrophages within the alveolar space may be the first cells to phagocytize nanoparticles and may further enhance the pro-inflammatory response as was seen in nanoparticle exposure to tungsten oxide nanoparticles and carbon nanotubes.[6,9,21] MoO_3 NPs agglomerates and/or aggregates were internalized in pulmonary macrophage vacuoles as demonstrated with TEM,

suggesting these nanoparticles were phagocytized. Smaller particles are able to penetrate the membrane of cells and become internalized while larger particles and aggregates may be phagocytized.[6]

Histopathological examination of lung tissue sections revealed focal hyperplasia of the airway epithelium and growths within the parenchyma following exposure to both MoO$_3$ NPs-treated groups. SEM revealed membrane blebbing and an increase in the presence of mucus on the surface of airway epithelium in both T-1 and T-7 groups. Such morphological changes suggest cellular injury following exposure to MoO$_3$ NPs. An increase in mucus production in airway has been seen following exposure to copper and silica oxide nanoparticles and is associated with inflammation and oxidative stress.[51] Ultrastructural morphology examined using TEM found autophagosome formation in macrophages from animals in the T-1 group. Formation of the double-membraned vesicle, the autophagosome, is the hallmark of autophagy, and can lead to autolysosome formation.[31] The T-7 group had damage to Type II pneumocytes as evident through a loss of lamellae in lamellar bodies. Gold nanoparticles have been shown to cause proliferation of Type II pneumocytes with degenerative lamellar bodies containing vacuoles as a result of oxidative stress and the inflammatory response.[52] SiO$_2$-SPION nanoparticles may be taken up in lamellar bodies but have been shown to cause damage and lead to the removal of damaged lamellar bodies through autophagy.[53]

The activation of the autophagic pathway may begin with the internalization of nanoparticles within the cell. The initiation of autophagy involves the Beclin-1/PI3K complex combining with the ULK/Atg1 complex causing the nucleation of the phagophore.[28,29] The protein expression of Beclin-1 was significantly increased in both animal groups exposed to MoO$_3$ NPs, suggesting that internalization of MoO$_3$ NPs can initiate the process of autophagy. The elongation of the phagophore to form the autophagosome involves LC3-I and the biomarker of autophagosome formation LC3-II. The protein expression of LC3-I and LC3-II showed no significant change in both animal groups exposed to 5 mg/m^3 MoO$_3$ NPs. A loss of LC3-II may indicate a blockage in the autophagy pathway and lead to a more severe acute lung injury.[33] LC3-II −/− mice exposed to copper oxide nanoparticles had a more severe lung injury when compared to wild-type mice.[33] Dysfunction or blockage in the autophagic pathway can be monitored through levels of P-62. The protein expression of P-62 in lung tissue from animals in the seven-day recovery group was significantly increased. An increase in levels of P-62 indicates that autophagic flux has been blocked or dampened following exposure to MoO$_3$ NPs. Interruptions in the autophagic flux may occur during: (1) autophagy induction and autophagosome formation, (2) inefficient autophagosome–lysosome fusion, or (3) inefficient degradation of materials in the autolysosome.[32] Over exposure to nanomaterial can result in excessive stimulation of autophagy leading to an increase in autophagosomes.[28] However, an increased number of autophagosomes does not indicate autophagy is functioning properly, but rather there may be a blockage in autophagic breakdown from the fusion of the autophagosomes to the lysosomes.[28] In the presence of

a lysosomal protease inhibitor, levels of LC3-II may remain unchanged, suggesting an accumulation of autophagosome from an inhibition of autophagosome–lysosome fusion.[54] Furthermore, when LC3-II formation is impaired, endogenous LC3-I can form puncta with P-62, and these puncta can accumulate when autophagic flux is impaired.[55] An intact and fully functioning lysosome is needed for autophagy to be carried out properly.[33] It has been shown that CuO NPs in combination with copper ion formation leads to lysosomal damage and a deficiency in the autophagic flux.[33] It is speculated that following internalization of MoO$_3$ NPs in the cytoplasm of the cell, particles may be internalized within the lysosome, and the acidic environment of the organelle may partially dissolve the particle to release the free ion of Mo. The toxicity noted may be a combination of both the free metal ion (Mo) and of the particle itself. MoO$_3$ NPs may impair autophagic flux by the free metal ion (Mo) inactivating the lysosomal enzymes leading to unchanged levels of LC3-II and/or by the nanoparticles damaging the membrane of the lysosome. Destabilized lysosomes would prevent their fusion with autophagosomes, thus leading to increased levels of P-62, indicating a possible interruption in the autophagic flux. Lysosomes with a loss of membrane integrity can lead to the release of cathepsin B that is an activator of the NLRP3 inflammasome.[24] Protein expression of cathepsin B was significantly increased in both animal groups exposed to 5 mg/m^3 MoO$_3$ NPs.

The NLRP3 inflammasome is a multiprotein complex seen in conditions such as asthma, chronic obstructive pulmonary disease (COPD), and pulmonary inflammation.[39] One mechanism in the activation of the NLRP3 inflammasome is the destabilization of the lysosome leading to the release of cathepsin B.[24] The components of the NLRP3 inflammasome were analyzed using immunoblots and ELISAs. The protein expression of NLRP3 was significantly increased in both animal groups exposed to 5 mg/m^3 MoO$_3$ NPs. During the oligomerization of the NRLP3 inflammasome, NRLP3 will interact with ASC's pyrin domain, and the CARD domain on ASC will recruit pro-caspase-1.[24] The levels of ASC were increased in animal groups exposed to 5 mg/m^3 MoO$_3$ NPs. The protein expression of caspase-1 was significantly increased in both treated groups exposed to 5 mg/m^3 MoO$_3$ NPs. Such data indicate the formation of the NLRP3 inflammasome. Pyroptosis involves the activation of caspase-1 resulting in an inflammatory process through the activation of IL-1β.[37] The levels of IL-1β were significantly increased in both groups exposed to 5 mg/m^3 MoO$_3$ NPs. While autophagy is known to remove activated NLRP3 complexes, an interruption in the autophagic flux may prevent the removal of such complexes leading to exaggerated levels of IL-1β.[36] In a study by Xiao et al.,[33] a loss of LC3-II expression was seen following exposure to copper oxide nanoparticles. This loss of LC3-II was accompanied by an increase in the mRNA expression of IL-1β and an exacerbation of acute lung injury.[33]

The activation of the NLRP3 inflammasome following exposure to nanomaterial has led to chronic granulomatous inflammation and fibrosis in the lung.[13,35,39] The subsequent production of IL-1β following inflammasome activation from exposure to nanoparticles has been shown
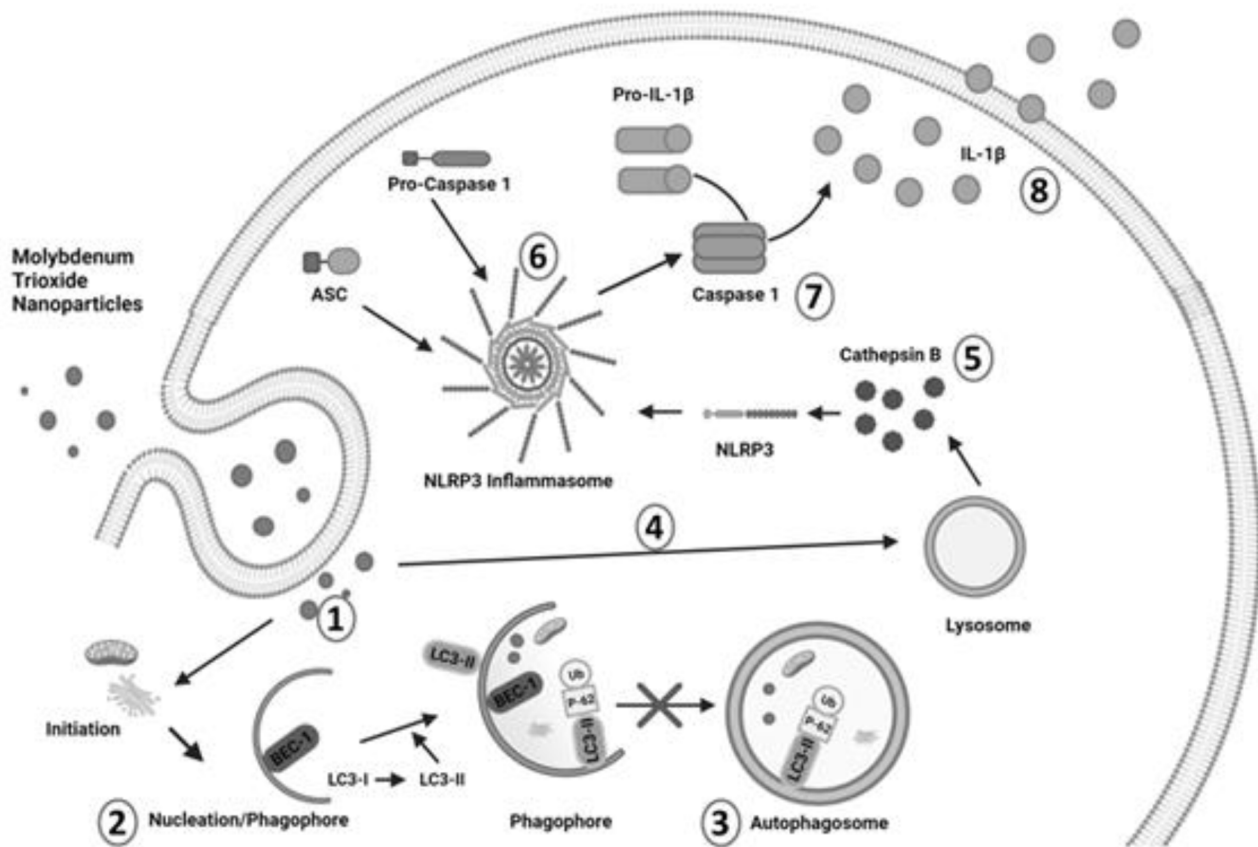
Figure 7. Representative proposed mechanism following pulmonary exposure to MoO_3 NPs. MoO_3 NPs are internalized in the cell (1) where the particles initiate autophagy through the nucleation of the phagophore via Beclin-1 (2). Unchanged LC3-I/II and increasing P-62 protein levels indicate an interruption in the autophagic flux and blockage of autophagosome formation (3). An alternative pathway (4) may be involved with internalization of MoO_3 NPs in the lysosome. An interruption in the autophagic flux through internalization of MoO_3 NPs destabilizes the lysosome releasing cathepsin B (5) and activates NLRP3. (6) Activated and oligomerization of the NLRP3 inflammasome, resulting in the activation of caspase-1 (7). Active caspase-1 causes the conversion of pro-IL-1β to IL-1β resulting in an inflammatory response, cellular damage, and cell death (8).

to lead to cross-talk among epithelial cells, macrophages, and fibroblasts followed by chronic collagen deposition in the lung.[38,56] This study indicated MoO_3 NPs activated the NLRP3 inflammasome and led to a significant increase in IL-1β levels. Multiple studies have shown activation of the NLRP3 inflammasome following exposure to nickel, tungsten, silica, cerium, titanium, and silver oxide nanoparticles, along with carbon nanotubes in environmental and occupational settings.[6,35,56]

It had been generally considered that MoO_3 NPs are deemed safe with low cytotoxicity, allowing the use of these nanoparticles to gain traction in consumer products and as chemotherapeutic agents.[2,57] When compared to aluminum, silver, and cadmium oxide nanoparticles, MoO_3 NPs were found to be the least cytotoxic in mammalian germline stem cells (C18-4 cell line) with an EC_{50} of 5 μg/mL[58] and more cytotoxic in rat liver cells (BRL 3A) compared to iron, tungsten, and manganese oxide nanoparticles with an EC_{50} of 171.5 μg/mL.[59] While there are some studies on the cytotoxicity of MoO_3 NPs in *in vitro* models, these studies lack data indicating the mechanism of toxicity. Currently, there is a lack of toxicological data on the cytotoxic potential of MoO_3 NPs in the respiratory system. While Mo is an essential trace metal and may not be considered as toxic as other metals, studies indicate the inhalation of Mo can lead to lung

damage. The inhalation of Mo fumes has been shown to cause irritation to the respiratory tract, pneumoconiosis, pulmonary hemorrhages, and damage to organs such as the kidney and liver.[3,11,12] This study has found that MoO_3 NPs are able to elicit an inflammatory response leading to cytotoxic effects within the respiratory system. More studies need to be carried out to evaluate the safety of these particles.

In summary (Figure 7) (created in biorender.com), the study investigated the toxic potential and the pulmonary response to inhaled MoO_3 NPs in the lungs of Golden Syrian Hamsters. The study determined MoO_3 NPs are internalized in lung tissue and macrophages following pulmonary exposure as was seen using TEM. The deposition of the particles within the lung may be responsible for initiating an inflammatory response. Increases in neutrophils from the BALF of animals exposed to MoO_3 NPs indicate that the lungs of these animals were undergoing an acute inflammatory response and seven days post exposure the inflammatory response shifted toward a chronic inflammation. The data suggest that following internalization of MoO_3 NPs, the nanoparticles initiate autophagy and the formation of the phagophore. However, MoO_3 NPs disrupt the autophagic flux interrupting the formation of the autophagosome and autolysosome. It is believed autophagy may not be at work following internalization of MoO_3 NPs, but rather an alternative pathway

with internalization of these particles in the lysosome. An internalization of MoO₃ NPs in the lysosome may lead to lysosomal destabilization and the release of cathepsin B. The interruption in the autophagic flux and subsequent release of cathepsin B is believed to be the mechanism activating the NLRP3 inflammasome. In combination with autophagy and pyroptosis, phagocytized and internalized MoO₃ NPs give rise to cellular damage through an inflammatory response. Conclusions to the activation of the NLRP3 inflammasome can be supported by previous work on inhaled tungsten oxide nanoparticles in Golden Syrian Hamsters.[6]

AUTHORS' CONTRIBUTIONS

E.A.H. carried out all experimentation. E.A.H. and J.M.C. designed the experiments and analyzed the data. Both authors contributed to editing and reviewing the manuscript.

DECLARATION OF CONFLICTING INTERESTS

The author(s) declared no potential conflicts of interest with respect to the research, authorship, and/or publication of this article.

ORCID IDS

Erin A Huber (iD) https://orcid.org/0000-0001-7122-902X

Joseph M Cerreta (iD) https://orcid.org/0000-0003-0361-3577

SUPPLEMENTAL MATERIAL

Supplemental material for this article is available online.

REFERENCES

1. Turnlund JR, Friberg LT. Molybdenum. In: Nordberg GF, Fowler BA, Nordberg M, Friberg LT (eds) *Handbook on the toxicology of metals*. 3rd ed. Oxford: Elsevier, 2007, pp.731–38
2. Odularu AT, Ajibade PA, Mbese JZ. Impact of molybdenum compounds as anticancer agents. *Bioinorg Chem Appl* 2019;**2019**:6416198–9
3. Barceloux DG. Molybdenum. *J Toxicol Clin Toxicol* 1999;**37**:231–7
4. Feng P, Cao W. Properties, application and synthesis methods of nano-molybdenum powder. *ACS Biomater Sci Eng* 2016;**4**:36–44
5. Dighore N, Jadhav S, Anandgaonker P, Gaikwad S, Rajbhoj A. Molybdenum oxide nanoparticles as antimicrobial agents. *J Clust Sci* 2016;**28**:109–18
6. Prajapati MV, Adebolu OO, Morrow BM, Cerreta JM. Evaluation of pulmonary response to inhaled tungsten (IV) oxide nanoparticles in golden Syrian hamsters. *Exp Biol Med (Maywood)* 2017;**242**:29–44
7. Sisler JD, Pirela SV, Shaffer J, Mihalchik AL, Chisholm WP, Andrew ME, Schwegler-Berry D, Castranova V, Demokritou P, Qian Y. Toxicological assessment of CoO and La2O3 oxide nanoparticles in human small airway epithelial cells. *Toxicol Sci* 2016;**150**:418–28
8. Srinivas A, Rao PJ, Selvam G, Murthy PB, Reddy PN. Acute inhalation toxicity of cerium oxide nanoparticles in rats. *Toxicol Lett* 2011;**205**:105–15
9. Rydman EM, Ilves M, Vanhala E, Vippola M, Lehto M, Kinaret PA, Pylkkänen L, Happo M, Hirvonen MR, Greco D, Savolainen K, Wolff H, Alenius H. A single aspiration of rod-like carbon nanotubes induces asbestos-like pulmonary inflammation mediated in part by the IL-1 receptor. *Toxicol Sci* 2015;**147**:140–55
10. Bonner JC. Nanoparticles as a potential cause of pleural and interstitial lung disease. *Proc Am Thorac Soc* 2010;**7**:138–41
11. Kapp RW. Molybdenum. In: Wexler P (ed.) Encyclopedia of toxicology. 3rd ed. Waltham, MA: Academic Press, 2014, pp.383–8
12. Vyskocil A, Viau C. Assessment of molybdenum toxicity in humans. *J Appl Toxicol* 1999;**19**:185–92
13. Ma J, Bishoff B, Mercer RR, Barger M, Schwegler-Berry D, Castranova V. Role of epithelial-mesenchymal transition (EMT) and fibroblast function in cerium oxide nanoparticles-induced lung fibrosis. *Toxicol Appl Pharmacol* 2017;**323**:16–25
14. Andujar P, Simon-Deckers A, Galateau-Sallé Fayard B, Beaune G, Clin B, Billon-Galland M, Durupthy O, Pairon J, Doucet J, Boczkowski J, Lanone S. Role of metal oxide nanoparticles in histopathological changes observed in the lung of welders. *Part Fibre Toxicol* 2014;**11**:2–13
15. Armstead AL, Arena CB, Li B. Exploring the potential role of tungsten carbide cobalt (WC-Co) nanoparticle internalization in observed toxicity toward lung epithelial cells in vitro. *Toxicol Appl Pharmacol* 2014;**278**:18
16. Miao J, Chard LS, Wang Z, Wang Y. Syrian Hamster as an animal model for the study on infectious diseases. *Front Immunol* 2019;**10**:2329–12
17. Bijlani KH, Sukhija HR, Cantor JO, Cerreta JM. Pulmonary inflammation induced by single walled carbon nanotubes in Golden Syrian Hamsters. *J Anal Pharm Res* 2016;**2**:1–13
18. Nakashima JM, Levin JR, Hyde DM, Giri SN. Repeated exposures to enzyme-generated oxidants cause alveolitis, epithelial hyperplasia, and fibrosis in hamsters. *Am J Pathol* 1991;**139**:1485–99
19. Michita RT, Mysorekar IU. Golden Syrian Hamsters as a model for revisiting the role of biological sex differences in SARS-CoV-2 infection. *Mbio* 2021;**12**:14
20. Bednash JS, Kagan VE, Englert JA, Farkas D, Tyurina YY, Tyurin VA, Samovich SN, Farkas L, Elhance A, Johns F, Lee H, Cheng L, Majumdar A, Jones D, Mejia OR, Ruane-Foster M, Londino JD, Mallampalli RK, Robinson RT. Syrian hamsters as a model of lung injury with SARS-CoV-2 infection: pathologic, physiologic, and detailed molecular profiling. *Transl Res* 2021;**240**:1–17
21. Chen Y, Yang Y, Xu B, Wang S, Li B, Ma J, Gao J, Zuo YY, Liu S. Mesoporous carbon nanomaterials induced pulmonary surfactant inhibition, cytotoxicity, inflammation and lung fibrosis. *J Environ Sci (China)* 2017;**62**:100–14
22. Peixoto MS, de Oliveira Galvão M, de Medeiros SRB. Cell death pathways of particulate matter toxicity. *Chemosphere* 2017;**188**:32–48
23. Manke A, Wang L, Rojanasakul Y. Mechanisms of nanoparticle-induced oxidative stress and toxicity. *Biomed Res Int* 2013;**2013**:942916
24. Yang Y, Wang H, Kouadir M, Song H, Shi F. Recent advances in the mechanism of NLRP3 inflammasome activation and its inhibitors. *Cell Death Dis* 2019;**10**:1–11
25. Mohammadinejad R, Moosavi MA, Tavakol S, Vardar DO, Hosseini A, Rahmati M, Dini L, Hussain S, Mandegary A, Klionsky DJ. Necrotic, apoptotic, and autophagic cell fates triggered by nanoparticles. *Autophagy* 2019;**15**:4–33
26. Feng X, Zhang Y, Zhang C, Lai X, Zhang Y, Wu J, Hu C, Shao L. Nanomaterial-mediated autophagy: coexisting hazard and health benefits in biomedicine. *Part Fibre Toxicol* 2020;**17**:1–26
27. Mizushima N, Yoshimorim T, Levine B. Methods in mammalian autophagy research. *Cell* 2010;**140**:313–26
28. Li T, Yang M. Vesicle trafficking, autophagy and nanoparticles: a brief review. *Current Nanomedicine* 2020;**10**:3–19
29. Kang R, Zeh HJ, Lotze MT, Tang D. The Beclin 1 network regulates autophagy and apoptosis. *Cell Death Differ* 2011;**18**:571–80
30. Vural A, Kehrl JH. Autophagy in macrophages: impacting inflammation and bacterial infection. *Scientifica (Cairo)* 2014;**2014**:825463–12
31. Liu Y, Levine B. Autosis and autophagic cell death: the dark side of autophagy. *Cell Death Differ* 2015;**22**:367–76
32. Zhang XJ, Chen S, Huang KX, Le WD. Why should autophagic flux be assessed? *Acta Pharmacol Sin* 2013;**34**:595–9
33. Xiao J, Tu B, Zhou X, Jiang X, Xu G, Zhang J, Qin X, Sumayyah G, Fan J, Wang B, Chen C, Zou Z. Autophagy deficiency exacerbates acute lung injury induced by copper oxide nanoparticles. *J Nanobiotechnology* 2021;**19**:1–18

34. Mishra AR, Zheng J, Tang X, Goering PL. Silver nanoparticle-induced autophagic-lysosomal disruption and NLRP3-inflammasome activation in HepG2 cells is size-dependent. *Toxicol Sci* 2016;**150**:473–87

35. Cho W, Duffin R, Howie SEM, Scotton CJ, Wallace WAH, MacNee W, Bradley M, Megson IL, Donaldson K. Progressive severe lung injury by zinc oxide nanoparticles; the role of Zn2+ dissolution inside lysosomes. *Part Fibre Toxicol* 2011;**8**:1–16

36. Li R, Ji Z, Qin H, Kang X, Sun B, Wang M, Chang CH, Wang X, Zhang H, Zou H, Nel AE, Xia T. Interference in autophagosome fusion by rare earth nanoparticles disrupts autophagic flux and regulation of an interleukin-1β producing inflammasome. *ASC Nano* 2014;**8**:10280–92

37. Bergsbaken T, Fink SL, Cookson BT. Pyroptosis: host cell death and inflammation. *Nat Rev Microbiol* 2009;**7**:99–109

38. Wang X, Sun B, Liu S, Xia T. Structure activity relationships of engineered nanomaterials in inducing NLRP3 inflammasome activation and chronic lung fibrosis. *Nanoimpact* 2017;**6**:99–108

39. Zheng R, Tao L, Jian H, Chang Y, Cheng Y, Feng Y, Zhang H. NLRP3 inflammasome activation and lung fibrosis caused by airborne fine particulate matter. *Ecotoxicol Environ Saf* 2018;**163**:612–9

40. Cantor JO. Bleomycin-induced pulmonary fibrosis. In: Cantor JO (ed.) CRC handbook of animal models of pulmonary disease. 1st ed. Boca Raton, FL: CRC Press, 1989, pp.115–27

41. Warner BM, Safronetz D, Kobinger GP. Syrian hamsters as a small animal model for emerging infectious diseases: advances in immunologic methods. In: Rezza G and Ippolito G (eds) Emerging and Re-emerging viral infections, **vol. 972**. Cham: Springer 2016, pp.87–101

42. Praphawatvet T, Peters JI, Williams RO. Inhaled nanoparticles – an updated review. *Int J Pharm* 2020;**587**:1–17

43. Ding S, Wang H, Wang M, Bai L, Yu P, Wu W. Resveratrol alleviates chronic "real-world" ambient particulate matter-induced lung inflammation and fibrosis by inhibiting NLRP3 inflammasome activation in mice. *Ecotoxicol Environ Saf* 2019;**182**:19

44. Lu X, Zhu T, Chen C, Liu Y. Right or left: the role of nanoparticles in pulmonary diseases. *Int J Mol Sci* 2014;**15**:17577–600

45. Warheit DB, Sayes CM, Reed KL, Swain KA. Health effects related to nanoparticle exposures: environmental, health and safety considerations for assessing hazards and risks. *Pharmacol Ther* 2008;**120**:35–42

46. Mourdikoudis S, Pallares RM, Thanh NTK. Characterization techniques for nanoparticles: comparison and complementarity upon studying nanoparticle properties. *Nanoscale* 2018;**10**:12871–934

47. Clogston JD, Patri AK. Zeta potential measurement. *Methods Mol Bio* 2011;**697**:63–70

48. Griffiths D, Bernt W, Hole P, Smith J, Malloy A, Carr B. Zeta potential measurement of nanoparticles by nanoparticle tracking analysis (NTA). *NSTI Nanotech* 2011;**1**:47

49. Jessop F, Trout KL, Holian A, Migliaccio C. Inflammatory cells of the lung: macrophages. Comprehensive toxicology. 3rd ed. Oxford: Elsevier, 2018

50. Jang D, Lee AH, Shin HY, Song HR, Park JH, Kang TB, Lee SR, Yang SH. The role of tumor necrosis factor alpha (TNF-α) in autoimmune disease and current TNF-α inhibitors in therapeutics. *Int J Mol Sci* 2021;**22**:1–16

51. Lim JO, Ko JW, Jung TY, Kim WI, Pak SW, Shin IS, Yun WK, Kim HC, Heo JD, Kim JC. Pulmonary inflammation caused by silica dioxide nanoparticles in mice via TXNIP/NLRP3 signaling pathway. *Mol Cell Toxicol* 2020;**16**:245–52

52. Elbakary RH, Okasha EF, Hassan Ragab AM, Ragab MH. Histological effects of gold nanoparticles on the lung tissue of adult male albino rats. *J Microsc Ultrastruct* 2018;**6**:116–22

53. Kononenko V, Erman A, Petan T, Križaj I, Kralj S, Makovec D, Drobne D. Harmful at non-cytotoxic concentrations: SiO2-SPIONs affect surfactant metabolism and lamellar body biogenesis in A549 human alveolar epithelial cells. *Nanotoxicology* 2017;**11**:419–29

54. Mizushima N, Yoshimori T. How to interpret LC3 immunoblotting. *Autophagy* 2007;**3**:542–5

55. Runwal G, Stamatakou E, Siddiqi FH, Puri C, Zhu Y, Rubinsztein DC. LC3-positive structures are prominent in autophagy-deficient cells. *Sci Rep* 2019;**9**:1–14

56. Gómez GDM, Urcuqui-Inchima S, Hernandez JC. Silica nanoparticles induce NLRP3 inflammasome activation in human primary immune cells. *Innate Immun* 2017;**23**:697–708

57. Tran AT, Krishnamoorthy K, Song YW, Cho SK, Kim SJ. Toxicity of nano molybdenum trioxide toward invasive breast cancer cells. *ACS Appl Mater Interfaces* 2014;**6**:2980–6

58. Braydich-Stolle L, Hussain S, Schlager JJ, Hofmann MC. In vitro cytotoxicity of nanoparticles in mammalian germline stem cells. *Toxicol Sci* 2005;**88**:412–9

59. Hussain SM, Hess KL, Gearhart JM, Geiss KT, Schlager JJ. In vitro toxicity of nanoparticles in BRL 3A rat liver cells. *Toxicol In Vitro* 2005;**19**:975–83